Key factors affecting graphene oxide transport in saturated porous media

Key factors affecting graphene oxide transport in saturated porous media

Ali Beryani[(1)(a)], Mohammad Reza Alavi Moghaddam[(1) (*)], Tiziana Tosco[(2)], Carlo Bianco[(2)], Seiyed Mossa Hosseini[(3)], Elaheh Kowsari[(1)], Rajandrea Sethi[(2)]

(1) Department of Civil and Environmental Engineering (CEE), Amirkabir University of Technology, Hafez Ave., 424, 15875-4413, Tehran, Iran
(2) Department of Environmental, Land and Infrastructure Engineering, Politecnico di Torino, Corso Duca degli Abruzzi 24 10129, Torino, Italy
(3) Physical Geography Department, University of Tehran, 16th Azar St., Enghelab Sq., 14155-6465, Tehran, Iran.

(a) Present address: Department of Environmental, Land and Infrastructure Engineering, Politecnico di Torino, Corso Duca degli Abruzzi 24 10129, Torino, Italy

(*) Corresponding author: alavi@aut.ac.ir, alavim@yahoo.com, tel. +98 021 64543008

Revised manuscript submitted to

Science of the Total Environment

July 2019

Abstract

This study focuses on the transport in porous media of graphene oxide nanoparticles (GONP) under conditions similar to those applied in the generation of *in-situ* reactive zones for groundwater remediation (i.e. GO concentration of few tens of mg/l, stable suspension in alkaline solution). The experimental tests evaluated the influence on GO transport of three key factors, namely particle size (300–1200 nm), concentration (10–50 mg/L), and sand size (coarse to fine). Three sources of GONP were considered (two commercial and one synthesized in the laboratory). Particles were stably dispersed in water at pH 8.5 and showed a good mobility in the porous medium under all experimental conditions: after injection of 5 pore volumes and flushing, the highest recovery was around 90%, the lowest around 30% (only for largest particles in fine sand). The particle size was by far the most impacting parameter, with increasing mobility with decreasing size, even if sand size and particle concentration were also relevant. The source of GONP showed a minor impact on the mobility. The transport test data were successfully modeled using the advection-dispersion-deposition equations typically applied for spherical colloids. Experimental and modeling results suggested that GONP, under the explored conditions, are retained due to both blocking and straining, the latter being relevant only for large particles and/or fine sand. The findings of this study play a key role in the development of an in-situ groundwater remediation technology based on the injection of GONP for contaminant degradation or sorption. Despite their peculiar shape, GONP behavior in porous media is comparable with spherical colloids, which have been more studied by far. In particular, the possibility of modeling GONP transport using existing models ensures that they can be applied also for the design of field-scale injections of GONP, similarly to other particles already used in nanoremediation.

Keywords:

Graphene oxide, transport in porous media, nanoparticle size effect, blocking, straining, nanoremediation

Highlights:

Graphene oxide transport is controlled by blocking and straining phenomena

Graphene oxide mobility in porous media strongly depends on its lateral size

A power law correlates the attachment/detachment coefficients to GO particle size

Good mobility/stability of GO makes it potentially capable in groundwater remediation

1. Introduction

Graphene oxide nanoparticles (GONP) are carbon-based irregular 2D flakes with a nanoscale thickness (Chen et al., 2012). GONP contain large amounts of oxygenated functional groups at the surface, such as carbonyl, carboxyl, hydroxyl, and phenol (Huang et al., 2011). They have been studied for several, diverse applications, e.g. in electronics, biomedicine, and sensors (Liu et al., 2013a; Novoselov et al., 2012; Qi et al., 2014a; Tortello et al., 2016). More recently, laboratory studies showed that GO can effectively remove several organic contaminants (Akpotu and Moodley, 2018; Iqbal and Abdala, 2013; Yang et al., 2013) and heavy metals (Jiang et al., 2018; Yin et al., 2019; Zhao et al., 2019; Zhou et al., 2016) from contaminated water. This evidence opens perspectives for several environmental applications, including wastewater treatment and in-situ remediation of contaminated aquifer systems, in particular for the removal of recalcitrant compounds and specific contaminants of concerns.

For the in-situ remediation the reference technology is the nanoremediation, that is, the injection of nanoparticles into the contaminated aquifer system for degradation, sorption precipitation or complexation of organic or inorganic contaminants (Corsi et al., 2018; Karn et al., 2009; O'Carroll et al., 2013; Patil et al., 2016; Tosco et al., 2014). The reactive particles must be dispersed and stably suspended in water-based slurries, thus allowing effective injection and targeting of the treatment area, which can be accomplished only with a strong control of the particle mobility in the porous medium. As a consequence, it is of pivotal importance to understand the main operative parameters controlling particle transport in the porous medium, and to develop reliable transport models to predict the particle mobility during injection and the final distribution of the reactive material. In this work, we study at a laboratory scale the potential injectability of GONP in the subsurface, which is a crucial aspect for the use of any nanoparticle for in situ treatment of a contaminated aquifer. In particular, we study how GONP transport in porous media is affected by those parameters which usually play a key role in nanoparticle injection for groundwater remediation, namely particle size and concentration, and porous medium size.

Compared to other materials already used for nanoremediation, eg. zero valent iron NPs, GONP inherently possess negative charges under a wide range of different environmental conditions, and can be easily dispersed in aqueous solutions, remaining suspended for a long period, even in the absence of stabilizers (Liu et al., 2013b; Qi et al., 2014a). Moreover, up to now most studies demonstrated that GONP tend to poorly interact with the porous medium, and therefore are retained on sand grains in limited amounts (Dong et al., 2016; Fan et al., 2015a; Feriancikova and Xu, 2012; Lanphere et al., 2013; Liu et al., 2013a; Liu et al., 2013c; Qi et al., 2014a; Sun et al., 2015; Xia et al., 2019). Thus, previous studies suggest a good potential mobility of GONP in aquifers and a relatively easy injectability at the field scale, compared to other nanoparticles already employed in the nanoremediation.

Until now, studies have been published on the suspension stability, transport and retention of GONP in porous media (Lanphere et al., 2014; Li et al., 2016; Liu et al., 2013b; Wang et al., 2017). However, they mostly focused on the influence of solution chemical parameters such as pH, ionic strength (IS), ion valence, and natural organic matter (NOM) concentration, which all play a key role on the long term fate of GONP in aquifer systems (Chrysikopoulos et al., 2017; Fan et al., 2015a; Fan et al., 2015b; Feriancikova and Xu, 2012; Jian-Zhou et al., 2015; Lanphere et al., 2013; Liu et al., 2013b; Liu et al., 2013c; Lu et al., 2017; Peng et al., 2017; Qi et al., 2014a; Xia et al., 2019). In particular, the influence of ion concentration and valence is now relatively well understood. Conversely, in this work we focus mainly on particle size and concentration and their physical interactions with porous media of different grain size; all these parameters become extremely relevant when particle suspensions are injected on purpose in the subsoil.

Particle size is known to play a critical role in colloid transport, as already elucidated by a broad literature, from colloid filtration theory and beyond. The porous medium grain size can have a huge impact on the colloid transport and retention, as predictable by the colloidal filtration theory (CFT) (Tufenkji and Elimelech, 2004; Yao et al., 1971). However, a direct extension of known processes and modeling approaches to GONP is not necessarily straightforward, due to the peculiar shape of such platelets. To the authors' knowledge, no previous study has already investigated and quantified the influence of particle size on GONP transport, and a few studies (Dong et al., 2019; Sun et al., 2012) have investigated the grain size effect on the transport and retention of GONP. Also, there is a lack of systematic information about the relationship between size of plate-like nanoparticles and their retention kinetic parameters. In this study, we consequently develop empirical equations expressing this relationship.

As a general rule, when colloidal suspensions are fairly stable and particles are sufficiently small compared to pore size to avoid straining and filtration phenomena, the injected concentration has a limited impact on particle transport, which is dominated by blocking phenomena (Tosco et al., 2014). This is the case of colloidal suspensions like bacteria, carboxylic latex, silica, titania and silver nanoparticles, and carbon nanotubes (Bradford and Bettahar, 2006; Bradford et al., 2009; Camesano and Logan, 1998; Godinez and Darnault, 2011; Kasel et al., 2012; Liang et al., 2013; Wang et al., 2012; Zhang et al., 2010). When considering the injection of particle suspensions for nanoremediation, graphene oxide is expected to be injected in relatively high concentrations (eg. several tens of mg/L) and then diluted in groundwater. In these conditions, the injected concentration often plays a major role in particle mobility and distribution in the porous medium. Sun et al. (2015) found that GONP mobility into sand-packed columns increased at higher input concentrations, coherently with the good colloidal stability of graphene oxide suspensions. In the present work, the impact of the injected concentration on GONP mobility is further studied, extending the range of conditions explored in the cited study.

In light of what discussed above, the aim of the present research is to elucidate unexplored or still unclear aspects related to GONP transport in porous media under conditions which could be expected for its application in nanoremediation, and to provide a reliable modeling framework able to correctly reproduce the observed processes. Column transport tests were performed using different graphene oxide types, particle size, injected concentration and sand samples. The experimental results were modeled using a well-established advection-dispersion-deposition equation for particle transport, using the numerical solution provided by the software MNMs (Bianco et al., 2016). Afterwards, the dependence of the model coefficients on the abovementioned parameters was quantified.

2. Materials and methods

2.1. GONP suspensions

In this study, three types of graphene oxide were used, identified as GO_1, GO_2, and GO_3 (Table 1). GO_1 (Graphenea Inc., Spain) is a single-layer graphene oxide dispersion, provided in a concentrated stock solution (4 g/L). GO_2 (Cheap Tubes Inc., US) is a single-layer GO provided in a dry powder ;from ,a stock solution (2 g/L) was then prepared by suspending the particles in DI water. GO_3 was synthesized in the laboratory following an eco-friendly improved Hummer's method developed by Chen et al. (2013), and stored in a stock solution at 1.45 g/L.

The synthesized GO_3 was characterized into details using the following methods: energy-dispersive X-ray spectroscopy (EDX, Octane SDD equipped with the SUTW detector, EDAX, United States), Fourier transform infrared spectroscopy (FT-IR, Bruker FTIR Equinox 55 spectroscopy, equipped with a MCT cryo-detector, Germany), X-ray diffraction (XRD, Equinox 3000, Inel, United States), Atomic Force Microscopy (AFM, NTEGRA AFMNT-MDT, NT-MDT Spectrum Instruments, Russia), and Field Emission Scanning Electron Microscopy (FE-SEM, Supra 40, ZEISS, Germany). The results of the characterization are reported in the Supporting Information. For the commercial GO_1 and GO_2 samples similar analyses were provided by the manufacturers (see SI for references).

Table 1: Characteristics of GO_1, GO_2, and GO_3

Name	Producer	Synthesis method	Size range after sonication (µm) (*)	Number of layers (**)	Thickness of layers (nm) (**)	Elemental analysis (***)			
						Carbon % (w/w)	Oxygen % (w/w)	Hydrogen % (w/w)	Sulfur % (w/w)
GO_1	Graphenea	Modified Hummer's method	0.3-1.6	1	0.8~1.2	49-56	41-50	0-1	2-4
GO_2	Cheap Tubes	Modified Hummer's method	0.3-0.8	1	0.7~1.2	35-42	45-55	3-5	-
GO_3	Own synthesis	Improved Hummer's method (without using $NaNO_3$)	0.9-1.5	1-2	0.8~2	45-60	40-55	-	<1

(*) DLS measurements
(**) AFM analysis for GO_3, manufacturers' data sheets for GO_1 and GO_2
(***) EDX analysis for GO_3, manufacturers' data sheets for GO_1 and GO_2

Size and zeta potential measurements were performed using dynamic light scattering (DLS) (Zetasizer Nano ZSP, Malvern Instruments, UK) for the three GO types.

For all tests, the GONP suspension was prepared immediately before injection by: diluting the stock solution to the desired GO concentration with DI water, applying probe sonication (UP200s Hielscher Ultrasound Technology, Germany), adding NaCl and NaOH to adjust, respectively, ionic strength (20 mM) and pH (8.5±0.5), and degassing in a vacuum chamber to remove residual air micro-bubbles. For GO_1 and GO_3, a different sonicating duration was used to adjust the average size of the particles (see detailed discussion on paragraph 3.1) and for GO_2 a 5 mins sonication was performed. The pH value was selected as typical value for GONP suspensions with good colloidal stability, which is therefore expected to be used in case of GO application to groundwater nanoremediation.

2.2. Porous medium

Silica sand with a minor content of K-feldspar (Sibelco, Dorfner, Germany) was sieved to obtain three different size ranges: coarse S_1 (0.3~1.0 mm, d_{50}=0.75 mm), medium S_2 (0.25~0.5 mm, d_{50}=0.4 mm), and fine S_3 (0.075~0.6 mm, d_{50}=0.28 mm). Prior to column packing, to remove fine suspended solids, metal oxides and other possible impurities, the sand was cleaned following the procedure reported in (Liu et al., 2013b; Qi et al., 2014a; Sun et al., 2015; Tosco et al., 2009). The zeta potential of the sand was measured (Zetasizer Nano ZSP, Malvern) following the method developed by Johnson et al. (1996). The measured values of zeta potential were -38±2, -40±1 and -42±2 mV for S_1, S_2, and S_3 in 20 mM NaCl solution at pH 8.5, respectively.

2.3. GONP transport tests

A Plexiglas cylinder (length 15.2 cm, inner diameter 1.6 cm) was wet-packed with degassed sand following the protocol detailed by Tosco et al. (2012). The column experiments were performed at a constant injection rate of 1.63×10^{-8} m^3/s, resulting in a Darcy velocity of 8.11×10^{-5} m/s. GONP suspensions were prepared following the protocol described in paragraph 2.1 at concentrations of 50, 20, 15 and 10 mg/L, representative of GONP concentrations applicable for field injections. The injection protocol involved the following steps:

- Pre-equilibration of the column with DI water for 5 pore volumes (PVs);
- Pre-flushing with background electrolyte solution (NaCl 20 mM) for 5 PVs;
- Injection of the GONP suspension in the background electrolyte solution for 4.5 PVs;
- Flushing with the background electrolyte solution for 4 PVs;
- Final flushing with DI water for 5 PVs (only for selected column tests).

During the experiments, salt and GONP concentrations were continuously measured at the column inlet and outlet using an UV-Vis Spectrophotometer (Specord S600, Analytik Jena, Germany) equipped with flow-through quartz cells with 5 mm light path (Hellma, Germany). The concentration was continuously monitored at a measurement frequency of 10 seconds at wavelengths of 198 nm (for dissolved species) and 230 nm (for GONP).

For each column test, the effective porosity (ε) and the dispersity (α) were determined via inverse fitting of the NaCl breakthrough curve (BTC), according to (Bianco et al., 2016). An average effective porosity of 0.49(±0.015), 0.47(±0.005), and 0.44(±0.015) and an average dispersity of 5.16(±0.784)×10^{-4} m, 4.87(±0.589)×10^{-4} m, and 3.97(±0.813)×10^{-4} m were obtained for the sands S_1, S_2, and S_3, respectively. The detailed results for each column test are reported in Table S1.

At the end of each column test, the sand column was dissected into five sections of 3 cm each to determine the profiles of retained GO mass and average particle size. The dissection procedure and the validation of concentration profiles against breakthrough curve mass balances are detailed in SI.

The GONP column transport tests were performed using different combinations of GO type (GO_1, GO_2, and GO_3), size and concentration, as well as different sand average size to systematically investigate the influence of these parameters on the transport of GONP.

2.4. GONP transport and retention modeling

The transport and retention of GONP in 1D saturated porous media was modeled using the general formulation of the advection-dispersion equation modified to include the particle mass exchange (deposition and release) between liquid and solid phase (Bradford and Bettahar, 2006; Bradford et al., 2003; Hosseini and Tosco, 2013; Qi et al., 2014a; Qi et al., 2014b; Tosco and Sethi, 2010; Wang et al., 2011) implemented in MNMs (https://areeweb.polito.it/ricerca/groundwater/software):

$$\begin{cases} \frac{\partial}{\partial t}(\varepsilon C) + \sum_i \left(\rho_b \frac{\partial S_i}{\partial t}\right) = -\frac{\partial}{\partial x}(qC) + \frac{\partial}{\partial x}\left(\varepsilon D \frac{\partial C}{\partial x}\right) \\ \rho_b \frac{\partial S_i}{\partial t} = f_i(C,S_i) = \varepsilon k_{a,i}\psi_i C - \rho_b k_{d,i} S_i \end{cases} \quad \text{(eq. 3)}$$

where C is the concentration of the nanoparticles in the liquid phase [M L^{-3}], t is time [T], ε is the medium porosity [-], i is a subscript regarding to the i^{th} interaction site, ρ_b is the bulk density of the porous medium [M L^{-3}], S_i is the mass concentration of nanoparticles deposited on the i^{th} site [M M^{-1}], x is the distance traveled from the inlet [L], q is Darcy flow rate [L T^{-1}], D is the dispersion coefficient [L^2 T^{-1}], $k_{a,i}$ and $k_{d,i}$ are the attachment and detachment kinetic coefficients, respectively [T^{-1}], and ψ_i is a function controlling the interaction dynamics of colloid deposition for i^{th} site.

In this study, a 2-site model considering two interaction mechanisms was used to describe particle interactions with the porous medium, namely, a physico-chemical attachment/detachment site with a maximum retainable concentration $S_{max,1}$ [M M^{-1}] (reversible blocking site, *i*=1) and a second site describing the physical retention of the nanoparticles (irreversible straining site, *i*=2). For the second interaction mechanism, the formulation proposed by Bradford et al. (2004; 2003) was adopted:

$$\psi_1 = \left(1 - \frac{S_1}{S_{max,1}}\right) \quad \text{(eq.2)}$$

$$\psi_2 = \left(1 + \frac{x}{d_{50}}\right)^{\beta_{str,2}} \quad \text{(eq.3)}$$

where d_{50} is the mean size of sand grains [L], and $\beta_{str,2}$ [-] is a kinetic exponent controlling the shape of the spatial distribution of retained nanoparticles.

The experimental breakthrough curves (BTCs) of GONP were fitted to the mathematical model using MNMs. The fitting parameters include the attachment/detachment kinetics ($k_{a,1}$, $k_{d,1}$, $k_{a,2}$) and the maximum retainable concentration $S_{max,1}$. The exponent $\beta_{str,2}$ was assumed equal to the value proposed in the literature (0.432) with good results (Bradford et al., 2003).

3. Results and discussions

3.1. Characterization of synthesized GONP (GO_3)

EDX analysis indicated that GO_1 and GO_3 contain similar percentages of C and O (Table 1). For GO_2 the produce reports a slightly higher content of C and lower of O. FT-IR transmission spectra confirmed for GO_3 the existence of epoxide (–O–), carbonyl (–C=O), carboxyl (–COOH) and hydroxyl (–OH) functional groups on the GO_3 surface (Figure S2). The XRD pattern of dried GO_3 showed a reflection peak at $2\theta=12°$, corresponding to d-space of 0.741 nm (Figure S3). This large interlayer spacing between the sheets implies the existence of oxygenated functional groups produced by the harsh chemical oxidation of pure graphite (with the smaller initial d-spacing of about 0.3 nm) and the formation of graphene oxide (Chen et al., 2013; Paulchamy et al., 2015; Shahriary and Athawale, 2014).

The specific surface area of the GO_3 (989 m^2/g) was estimated using the methylene blue titration method proposed by Montes-Navajas et al. (2013). The experimental procedure and calculations of specific surface area are detailed in the SI (Figure S4).

AFM analysis indicated that the synthesized GO_3 suspension (in DI, after 45 seconds ultra-sonication) consisted of single- or two-layer flakes with thickness 0.8~2 nm (Figure S5) and lateral size of 500~1000 nm. AFM analysis of GO_2 provided by the manufacturer evidenced a similar thickness (up to 3 nm). FE-SEM analysis also showed that the lateral size of GO_3 after synthesis (without size adjustment) ranged between 900~1500 nm (Figure S6).

GONP formed stable colloidal suspensions: kinetic aggregation measurements using DLS (Figure S7) and visual sedimentation tests (not reported) indicated that the three GONP were all stably dispersed in a 20 mM NaCl solution for at least two hours (i.e. longer than the duration of the transport tests). This is in agreement with the strongly negative values of Zeta potential measured for the suspensions (-50±4, -55±6, and -56±1 mV for GO_1, GO_2, and GO_3, respectively).

It was observed that applying probe sonication for a different duration the average size of the GONP in suspension changes: the longer the duration, the smaller the average size (Figure

S8). Particle size distribution is broader if no sonication is applied, or applied for short durations, and becomes narrower when sonication is prolonged (3 mins or higher). Sonication did not significantly alter other properties of the GONP (colloidal stability and zeta potential, compare Figure S9). Consequently, based on these results, the average size of GO_1 and GO_3 (Table 2) was controlled by changing the duration of probe sonication during the suspension preparation, following Figure S8.

It is worth to mention that, due to their platelet-like shape, GONP size measurements obtained from DLS cannot be directly interpreted as the correct size of the particles, and are rather related to both platelet lateral size, shape and thickness, as discussed in the literature (Lotya et al., 2013). Consequently, in this work the measured average size values were used as a semi-quantitative measurement of the lateral size, and changes in average size were analyzed mainly in terms of particle size increase/decrease, rather than absolute values. The actual lateral size was instead obtained from SEM and AFM measurements (see Supporting Information).

3.2. Column transport tests

The GONP column transport tests were performed using different combinations of GO type (GO_1, GO_2, and GO_3), lateral size and concentration, as well as different sand average size to systematically investigate the influence of these parameters on the transport of graphene oxide (Table 2). The observed and simulated BTCs were normalized to the injected concentration (C/C_0) and reported as a function of pore volumes (Figure 1, Figure 4, and Figure 6). In the graphs, P.V. = 0 (time t = 0) corresponds to the beginning of GO injection, thus equilibration and pre-flushing steps are not reported. The retention profiles were reported as a normalized concentration of deposited GONP (S, namely mass of GONP normalized to the sand mass) (Figure 2, Figure 5, and Figure 7).

The experimental BTCs were fitted using the 2-site retention model equations (1-3). As a general rule, the results indicated that under the tested experimental conditions the model equations can satisfactorily simulate the observed BTCs of GONP (for all the experiments R^2>0.99) with a very little mismatch in both rising and tailing parts of the BTCs. For GO_2 only, in some cases, the second site (straining) had a negligible effect on the particle transport and was therefore removed. The fitted model parameters are summarized in Table 2.

The low values of $k_{d,1}$ (detachment coefficient for blocking deposition) obtained for all the tests indicated that physico-chemical deposition will be practically irreversible if the ionic strength (and therefore the particle-collector electrostatic interactions) is not modified. This is coherent with the negligible tailing observed in the experimental breakthrough curves. A few additional tests were performed flushing the columns after particle deposition with stepwise decreasing salt concentration. The results (Figure S10) revealed that particles retained due to physical-chemical interactions are not readily mobilized unless a strong decrease in salt concentration is applied (in our experiments, NaCl concentration below 5 mM).

Table 2: Experimental conditions of column transport tests and fitted coefficients ($k_{a,1}$, $k_{d,1}$, $S_{max,1}$, and $k_{a,2}$)

Test No.	GO Type	C_0 (mg/L)	GO Size (nm)	Sand	$k_{a,1}$ [s^{-1}]	$k_{d,1}$ [s^{-1}]	$S_{max,1}$ [g/g]	$k_{a,2}$ [s^{-1}]
1	GO_1	50	898±47	Coarse	$6.06\cdot10^{-4}$	$8.34\cdot10^{-5}$	$5.38\cdot10^{-6}$	$4.70\cdot10^{-4}$
2		50	1000±49	Medium	$1.20\cdot10^{-3}$	$8.18\cdot10^{-6}$	$4.79\cdot10^{-6}$	$1.90\cdot10^{-3}$
3		50	984±55	Fine	$2.30\cdot10^{-3}$	$3.54\cdot10^{-5}$	$9.00\cdot10^{-6}$	$3.10\cdot10^{-3}$
4		20	1128±111	Coarse	$9.07\cdot10^{-4}$	$5.00\cdot10^{-5}$	$3.25\cdot10^{-6}$	$1.40\cdot10^{-3}$
5		20	1100±63	Medium	$2.50\cdot10^{-3}$	$3.20\cdot10^{-5}$	$5.36\cdot10^{-6}$	$2.40\cdot10^{-3}$
6		20	1076±59	Fine	$2.44\cdot10^{-3}$	$2.92\cdot10^{-5}$	$4.90\cdot10^{-6}$	$5.28\cdot10^{-3}$
7		15	1122±72	Fine	$2.90\cdot10^{-3}$	$1.81\cdot10^{-5}$	$4.93\cdot10^{-6}$	$6.20\cdot10^{-3}$
8		10	1082±69	Fine	$3.60\cdot10^{-3}$	$5.47\cdot10^{-5}$	$3.46\cdot10^{-6}$	$8.90\cdot10^{-3}$
9		20	1286±332	Fine	$4.08\cdot10^{-3}$	$2.34\cdot10^{-5}$	$4.72\cdot10^{-6}$	$9.30\cdot10^{-3}$
10		20	980±40	Fine	$2.51\cdot10^{-3}$	$3.46\cdot10^{-5}$	$5.44\cdot10^{-6}$	$5.70\cdot10^{-3}$
11		20	820±70	Fine	$1.88\cdot10^{-3}$	$3.49\cdot10^{-5}$	$4.87\cdot10^{-6}$	$2.63\cdot10^{-3}$
12		20	595±30	Fine	$1.70\cdot10^{-3}$	$4.60\cdot10^{-5}$	$5.34\cdot10^{-6}$	$8.95\cdot10^{-4}$
13		20	530±30	Fine	$1.64\cdot10^{-3}$	$5.50\cdot10^{-5}$	$5.56\cdot10^{-6}$	$9.87\cdot10^{-4}$
14		20	380±20	Fine	$1.60\cdot10^{-3}$	$5.80\cdot10^{-5}$	$4.23\cdot10^{-6}$	$7.27\cdot10^{-4}$
15	GO_2	50	417±15	Coarse	$9.50\cdot10^{-4}$	$5.64\cdot10^{-5}$	$9.88\cdot10^{-6}$	$3.73\cdot10^{-4}$
16		50	388±20	Medium	$1.30\cdot10^{-3}$	$6.33\cdot10^{-5}$	$8.20\cdot10^{-6}$	$6.82\cdot10^{-4}$
17		50	380±8	Fine	$2.61\cdot10^{-3}$	$1.02\cdot10^{-5}$	$1.38\cdot10^{-5}$	$1.40\cdot10^{-3}$
18		20	362±21	Coarse	$1.60\cdot10^{-3}$	$5.09\cdot10^{-5}$	$5.79\cdot10^{-6}$	-
19		20	393±14	Medium	$8.64\cdot10^{-4}$	$3.41\cdot10^{-5}$	$4.48\cdot10^{-6}$	-
20		20	370±16	Fine	$2.75\cdot10^{-3}$	$2.45\cdot10^{-5}$	$1.12\cdot10^{-5}$	-
21		15	448±54	Fine	$2.70\cdot10^{-3}$	$1.80\cdot10^{-5}$	$1.07\cdot10^{-5}$	-
22		10	409±44	Fine	$4.25\cdot10^{-3}$	$1.34\cdot10^{-5}$	$8.98\cdot10^{-6}$	-
23	GO_3	50	687±24	Coarse	$7.76\cdot10^{-4}$	$1.13\cdot10^{-4}$	$8.41\cdot10^{-6}$	$5.43\cdot10^{-5}$
24		50	679±19	Medium	$1.10\cdot10^{-3}$	$8.22\cdot10^{-5}$	$8.15\cdot10^{-6}$	$9.82\cdot10^{-4}$
25		50	727±28	Fine	$2.10\cdot10^{-3}$	$4.60\cdot10^{-5}$	$8.04\cdot10^{-6}$	$1.90\cdot10^{-3}$
26		20	650±15	Coarse	$1.10\cdot10^{-3}$	$4.03\cdot10^{-5}$	$4.83\cdot10^{-6}$	$1.50\cdot10^{-3}$
27		20	677±21	Medium	$1.80\cdot10^{-3}$	$3.51\cdot10^{-5}$	$7.03\cdot10^{-6}$	$1.40\cdot10^{-3}$
28		20	733±43	Fine	$1.90\cdot10^{-3}$	$4.04\cdot10^{-5}$	$4.37\cdot10^{-6}$	$3.70\cdot10^{-3}$
29		15	645±27	Fine	$3.60\cdot10^{-3}$	$5.47\cdot10^{-6}$	$3.46\cdot10^{-6}$	$8.90\cdot10^{-3}$
30		10	588±28	Fine	$4.60\cdot10^{-3}$	$1.02\cdot10^{-5}$	$5.45\cdot10^{-6}$	$8.40\cdot10^{-3}$
31		20	1167±111	Fine	$2.80\cdot10^{-3}$	$2.74\cdot10^{-5}$	$6.24\cdot10^{-6}$	$8.60\cdot10^{-3}$
32		20	868±41	Fine	$2.00\cdot10^{-3}$	$3.44\cdot10^{-5}$	$5.65\cdot10^{-6}$	$3.30\cdot10^{-3}$
33		20	450±15	Fine	$1.49\cdot10^{-3}$	$4.82\cdot10^{-5}$	$5.21\cdot10^{-6}$	$1.09\cdot10^{-3}$
34		20	270±60	Fine	$1.30\cdot10^{-3}$	$6.33\cdot10^{-5}$	$4.36\cdot10^{-6}$	$8.71\cdot10^{-4}$

3.2.1. Effect of lateral size and type of GONP

For a given GO type, the average lateral size was adjusted by tuning the duration of the probe sonication prior injection, following Figure S8. Figure 1 and Figure 2 report the experimental and simulated BTCs and the measured retention profiles in columns packed with fine sand (S_3) for different lateral sizes of GO_1 (tests no. 6 and 9-14) and GO_3 (test no. 28, 31-34) in the range 300 to 1300 nm. The results revealed that the GO size strongly affects retention and transport in saturated sand columns. The mobility of GONP tends to increase with decreasing particle size. Mass balances (Table S1) indicate that the percentage of retained particles decreases with decreasing the GO size, consistently with results reported by previous studies for other types of particles, e.g. the work of Hu et al. (2017) for spherical carbon nanoparticles. Thus, it suggests that particle shape, for our GONP, has no major influence in this sense. However, a better insight into retention mechanisms is necessary.

Figure 2a shows that larger GO_1 produces strongly declining retention profiles, while smaller GO_1 produces a more uniform distribution along the column. Previous studies mainly observed GONP retention to be dominated by physical-chemical interactions with the porous matrix, resulting in blocking phenomena (Dong et al., 2019; Dong et al., 2016; Dong et al., 2017; Feriancikova and Xu, 2012; Liu et al., 2013b; Sun et al., 2015; Wang et al., 2018; Xia et al., 2019). In our study we observed the same behavior for small particles, while for the largest ones (close to or exceeding 1 micron) the declining retention profiles suggest that physical retention also plays an important role. Particle size analysis on retained particles (Figure S11) showed that, for these tests, larger particles are retained close to the column inlet, and smaller ones travel longer distances; conversely, an almost constant size distribution was observed when particles significantly smaller than 1 micron were injected.

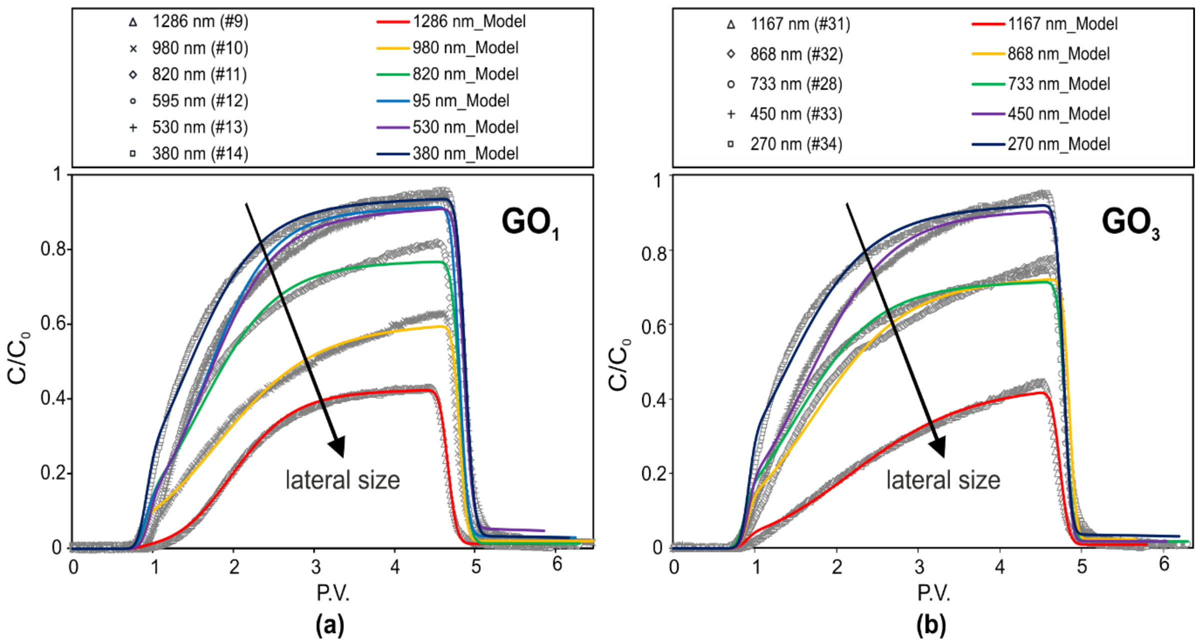

Figure 1: Observed and simulated breakthrough curves (BTCs) of (a) GO_1 and (b) GO_3 with different lateral sizes at the same input concentrations of 20 mg/L in Sand S_3. Symbols: experimental data/ Lines: simulation results

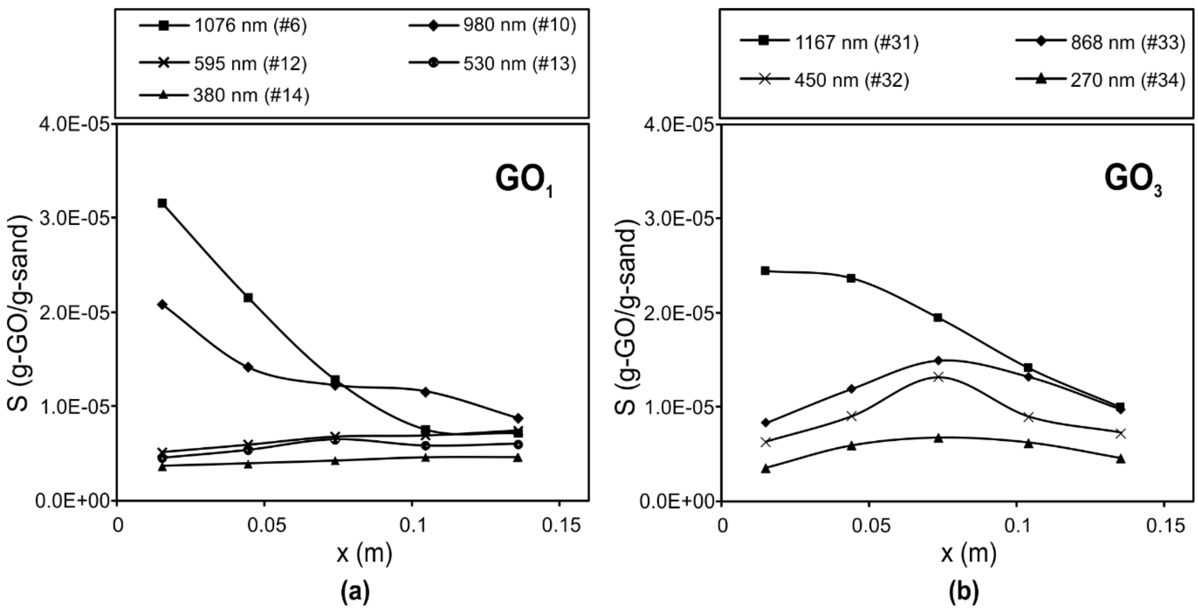

Figure 2: Observed retention profiles of (a) GO_1 and (b) GO_3 with different lateral sizes at the same input concentrations of 20 mg/L in Sand S_3

Likely, the discussed behavior can be attributed to straining. This result is consistent with a previous study (Qi et al., 2014a) where the significant straining effect was reported for heterogeneous (natural) saturated porous media. For rounded-shape colloids, it is commonly accepted that straining is a relevant process if the ratio of particle (d_p) to finer sand size (d_{10}) $d_p/d_{10} > 0.008$ (Xu et al., 2006). For our sand S_3 (having d_{10} = 75 μm) this corresponds to GONP of approximately 600 nm. As an evidence, clearly declining profiles were observed for particles of 1 μm or larger, corresponding to a ratio $d_p/d_{10} \geq 0.013$.

For GO_3 (Figure 2b) a quite uncommon trend was obtained, with higher retention in the central portion of the column. This is particularly evident for particles with intermediate size, probably due to the relatively broad size distribution of these samples (Figure S8 II-b). Similar non-monotonic trends have been recently attributed to competing deposition of non-monodispersed colloids in fractures (Malgaresi et al., 2019). This trend was less evident for the smallest particles (270 nm) with a fairly sharp particle size distribution, which tended to produce more uniform retention profiles. For the largest ones (1167 nm) instead, a strongly declining trend was observed due to the predominant effect of straining which masked the competition effect.

The fitted values of the model parameters (namely, $k_{a,1}$, $S_{max,1}$, $k_{d,1}$, $k_{a,2}$) are reported in Table 2 and Figure 3. Fitted values of $S_{max,1}$ oscillate in the range of $3.5\text{-}6.0 \cdot 10^{-6}$ g/g (Figure 3b), without any evident correlation between $S_{max,1}$ and GO lateral size (d_p). This range is comparable with the retained concentrations (S) measured for small particles (Figure 2) when straining does not play a significant role. The attachment kinetics $k_{a,1}$ and $k_{a,2}$ both increase with increasing particle size d_p (Figure 3a and c). Increasing $k_{a,1}$ with d_p means that smaller GONP attach to the retention site 1 more slowly than larger ones, even if they all tend to reach a similar saturation concentration. This is also reflected by the different steepness of breakthrough curves for small particles in Figure 1.

Similar to $k_{a,1}$, the parameter $k_{a,2}$ increases with increasing d_p. For small particles, $k_{a,1}$ and $k_{a,2}$ are similar. Conversely, when straining becomes relevant, $k_{a,2}$ significantly exceeds $k_{a,1}$ and retention due to blocking becomes negligible compared to straining. In this case, retention profiles are strongly declining along the column and breakthrough curves tend to a plateau concentration C/C_0 lower than 1, which represents an irreversible straining.

An empirical power function can be used to model the correlation of the three parameters ($k_{a,1}$, $k_{d,1}$ and $k_{a,1}$) with d_p:

$$k_i = a + b\, {d_p}^c \tag{4}$$

where k_i is the generic attachment/detachment kinetic coefficient, and a, b, and c are fitting parameters. For $k_{a,1}$ the fitted values are a = $1.41 \cdot 10^{-3}$ s^{-1}, b = $3.10 \cdot 10^{15}$ $(s \cdot m)^{-1}$, c = 3.077 with R^2 = 0.938; for $k_{a,2}$ a = $6.14 \cdot 10^{-4}$ s^{-1}, b = $1.20 \cdot 10^{15}$ $(s \cdot m)^{-1}$, c = 2.905 with R^2 = 0.947; for $k_{d,1}$ a = $4.37 \cdot 10^{-7}$ s^{-1}, b = $1.28 \cdot 10^{-8}$ $(s \cdot m)^{-1}$, c = -0.567 with R^2 = 0.915. The fitted curves are reported in Figure 3a-c as solid lines. The fitting is satisfactory for all coefficients, with R^2 values above 0.93 in all three cases. It is worth to notice that for all kinetic coefficients the value represents the lowest, asymptotic kinetics for small (in case of attachment) or large (in case of detachment) particles. A very similar exponent, close to 3, is found for $k_{a,1}$ and $k_{a,2}$. The exponent for $k_{d,1}$ is negative reflecting the declining trend of the detachment kinetics with increasing particle size.

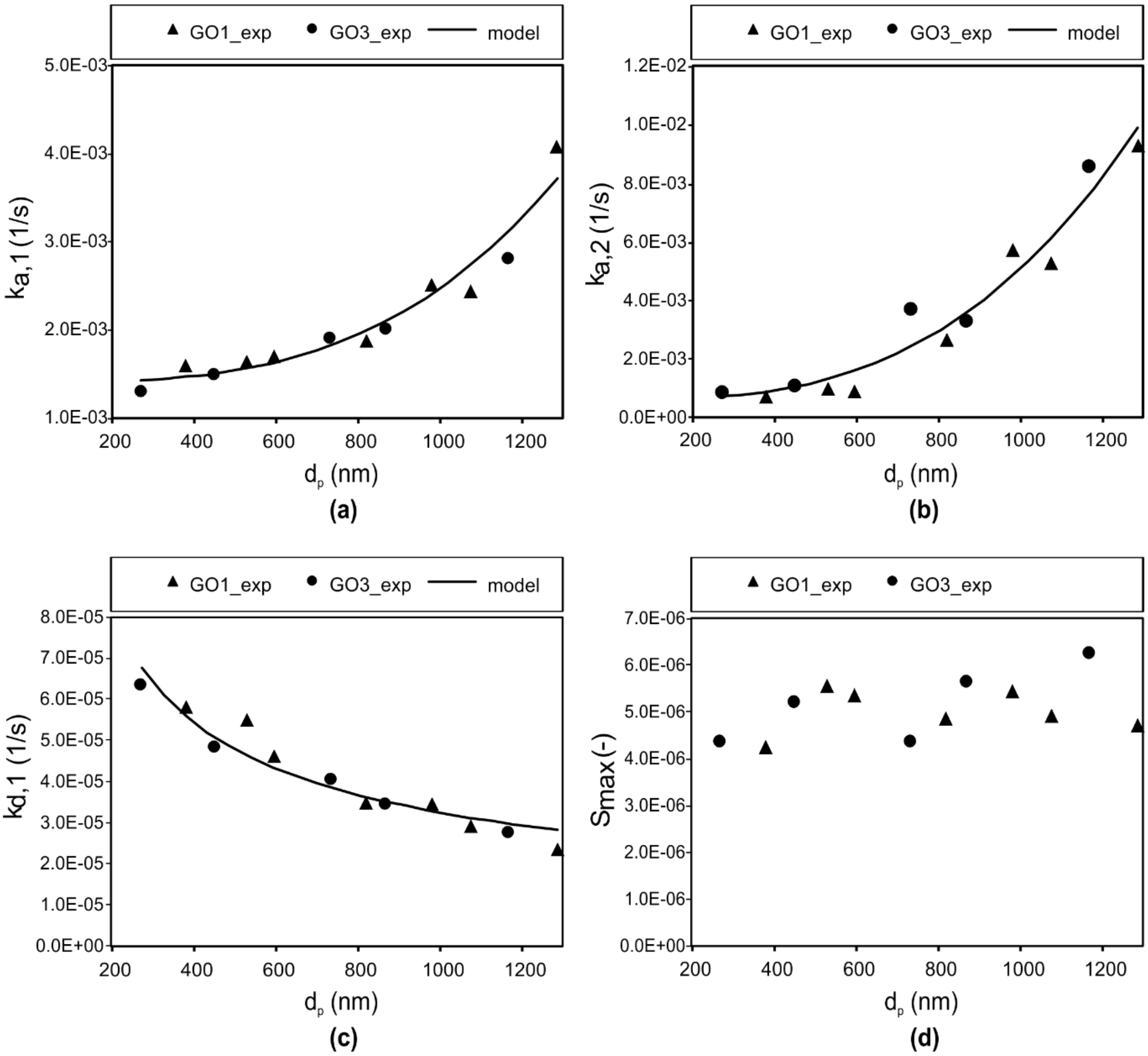

Figure 3: GONP deposition and release coefficients as a function of average particle size for GO_1 and GO_3: (a) $k_{a,1}$ (b) $k_{a,2}$ (c) $k_{d,1}$ and (d) S_{max}

Interestingly, the results were very close to previous findings obtained for rounded-shaped colloids. The obtained trends of $k_{a,2}$ versus d_p are consistent with Bradford et al. (2003) who reported that a power function can represent a good correlation between $k_{a,2}$ and particle size for latex microparticles. Moreover, the exponent obtained from the detachment kinetic coefficient (-0.567) is very close to the theoretical value of -0.58 proposed by Rittman (1982) and later adopted by Brovelli et al. (2009) for the detachment of biofilms. However, further studies would be needed to understand if the empirical law of equation 4, or similar power functions, can be generalized to any type of particles.

3.2.2. Effect of input concentration

The transport tests at different input mass concentration (C_0) were performed in columns packed with sand S_3 (tests no. 3 and 6-8 for GO_1, n. 17 and 20-22 for GO_2, n. 25 and 28-30 for GO_3, see Table 2). The GONP size is constant for each test performed with the same GO type but different sizes were selected for GO_1, GO_2, and GO_3, in order to have a set of tests where, respectively, straining is relevant (for GO_1, average size close to 1 μm), is not relevant (GO_2, approximately 400 nm) and is expected to play a role, but not to dominate transport (GO_3, 700 nm).

The breakthrough curves (Figure 4) show similar trends for all three types of GONP: changing the input concentration in the range of 10 to 50 mg/L affected the transport and retention of the nanoparticles. The mobility of all types of GO tends to increase with increasing the injected concentration C_0. This finding is consistent with Sun et al. (2015), the only previous study, to our knowledge, investigating the influence of inlet concentration on the transport and retention of GONP. Mass balance and mass recovery calculations (Table S1) confirm that the total retained mass decreases with increasing C_0. The observed behavior is coherent with blocking-dominated deposition. In other words, a higher C_0 saturates the deposition sites more rapidly compared with lower C_0, thus increasing the overall mobility of the injected suspension. Our tests with higher C_0 show a steeper increase of the breakthrough curves, even if the effect is less pronounced for GO_2, which is the sample with the overall highest mobility and smallest particle size. It is noteworthy that some differences exist among the GO types. However, based on the results discussed in the previous paragraph, it can be assumed that these differences are related mainly to the different size of the three samples, rather than to possible minor differences in composition and surface properties.

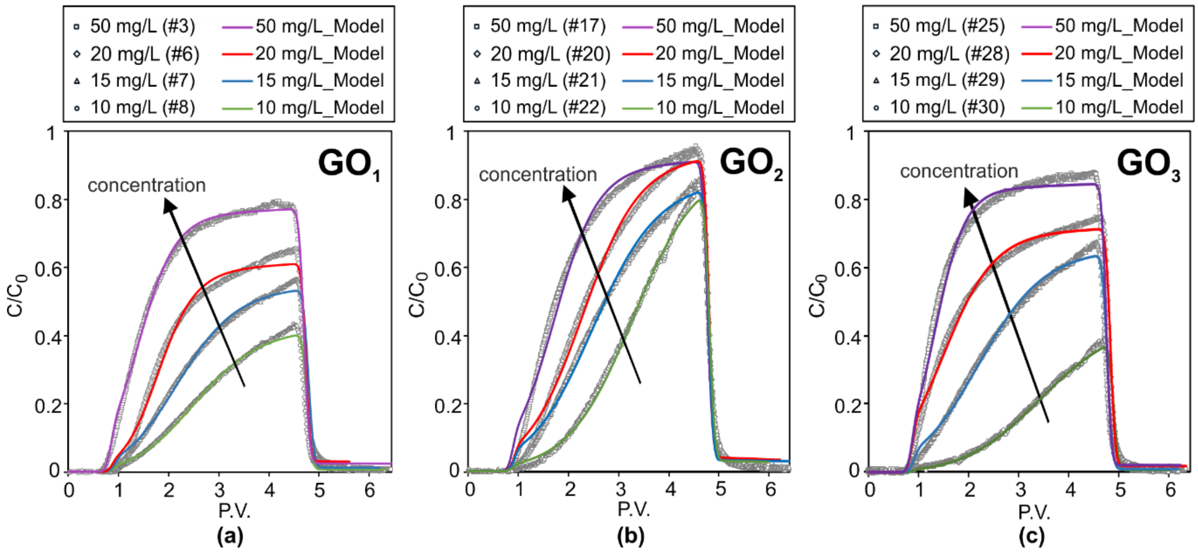

Figure 4: Observed and simulated breakthrough curves (BTCs) of (a)GO_1 (Z-Ave. 1050±100 nm), (b) GO_2 (Z-Ave. 410±50 nm), and (c) GO_3 (Z-Ave. 650±100 nm) at different input concentrations from 50 mg/L to 10 mg/L in sand S_3. Symbols: experimental data/ Lines: simulation results

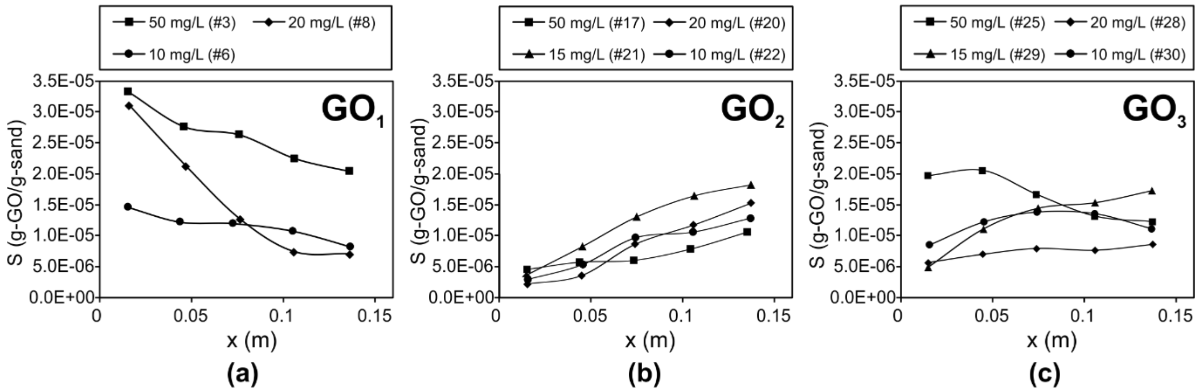

Figure 5: Observed retention profiles of (a) GO_1, (b) GO_2, and (c) GO_3 at different input concentrations from 50 mg/L to 10 mg/L in sand S_3.

Considering the modeling of GONP transport, the fitting obtained is satisfactory for all breakthrough curves. For GO_1 and GO_3, the two-site deposition model correctly describes the GO transport. Conversely, for GO_2, characterized by the smallest particle size, straining is irrelevant for all tests except those where the highest concentration (50 mg/L) is injected. This suggests that, in such conditions, a stronger interaction arises between deposited particles and those suspended in the pore water, promoting enhanced deposition processes.

The attachment and detachment kinetic coefficients $k_{a,1}$ and $k_{d,1}$ do not significantly change with changing injected concentration. Conversely, a slight increase of $S_{max,1}$ with increasing injected concentration is observed, even if the explanation for this is unclear, and further investigation would be needed to elucidate this aspect.

3.2.3. Effect of sand grain size

Figure 6 depicts the experimental and simulated BTCs of GO_1 (tests n. 1-6 in Table 2) injected at 20 and 50 mg/L in sands S_1 (coarse), S_2 (medium) and S_3 (fine). The corresponding retention profiles are reported in Figure 7. Also, for this set of tests, the size of the three GO samples was adjusted to approximately 1 μm for GO_1, 400 nm for GO_2 and 700 nm for GO_3.

The results indicate that the sand grain size significantly affects the transport and retention of GONP. The same tests performed using GO_2 (tests 15-20 in Table 2) and GO_3 (tests 23-28 in Table 2) are reported in the Supporting Information (Figure S13) and show similar results. The impact of sand size on the transport of GO_2 and GO_3 showed similar results.

As a general outcome, the mobility of GONP at a given C_0 tends to increase with increasing the sand grain size. The highest breakthrough concentration is found in coarse sand. The corresponding retention profile is almost constant along the column, thus indicating that straining is limited or even negligible. Conversely, reducing the grain size, the breakthrough decreases, and straining becomes more relevant. The mass balances (Table 1) confirm that decreasing the sand size lead the total retention to significantly increase for all GO types and both injected concentrations.

The fitted parameters reported in Table 2 indicate how changing the sand size affects the relative importance of blocking and straining retention mechanisms. As for physical-chemical deposition following the blocking dynamics, the attachment kinetic coefficient $k_{a,1}$ increases with decreasing sand size (from S_1 to S_3), and coherently $k_{d,1}$ decreases for both injected concentrations. This was expected from the established literature on colloid removal efficiency in granular media (Messina et al., 2016; Sun et al., 2015; Tufenkji and Elimelech, 2004; Yao et al., 1971). Some other experimental studies investigating the effect of the grain size on the particle attachment rate (Bradford and Bettahar, 2006; Kasel et al., 2012; Liang et al., 2013; Sun et al., 2015; Torkzaban et al., 2010) achieved the similar results, even if the great majority of such studies focused on spherical colloidal particles, e.g. carboxyl latex, QDs, and AgNPs.

Differences in the maximum retainable concentration due to physico-chemical interactions ($S_{max,1}$) among the three sand samples are attributable to differences in SSA, since no significant difference in zeta potential was observed. As a general rule, the fitted values of $S_{max,1}$ (Table 2) increase with decreasing sand size (i.e. from S_1 to S_3) for a given GO type and injected concentration; this results in $S_{max,1}$ values for S_3 approximately two times higher than the $S_{max,1}$ obtained for S_1, in agreement with SSA of sand grains (assuming spherical grains, SSA for S_1 and S_3 is respectively 0.008 and 0.003 m^2/kg, being the average grain size 0.75 and 0.28 mm).

Straining also contributed to the retention of GONP and affected the shape of profiles of retained particles. Based on the considerations discussed in the previous paragraphs, straining is expected to occur for GO_1 and, limitedly, for GO_2. Back again to the ratio d_p/d_{10} and the straining limit of 0.008 (Xu et al., 2006), GO_1 was expected to exceed this threshold value in sand S_3, and to approach the limit for S_2. Coherently, the retention profiles (Figure 7) showed a steep decrease for S_3 and a less pronounced decrease for S_2. The fitted straining coefficients $k_{a,2}$ are lower for coarse sand and increase with decreasing sand size. Changes in $k_{a,2}$ from S_1 to S_3 cover approximately one order of magnitude (typically from 10^{-4} s^{-1} to 10^{-3} s^{-1}) and are more evident at the highest injected concentration (for example, compare the values of $k_{a,2}$ for GO_1 and GO_3 injected at 50 mg/L).

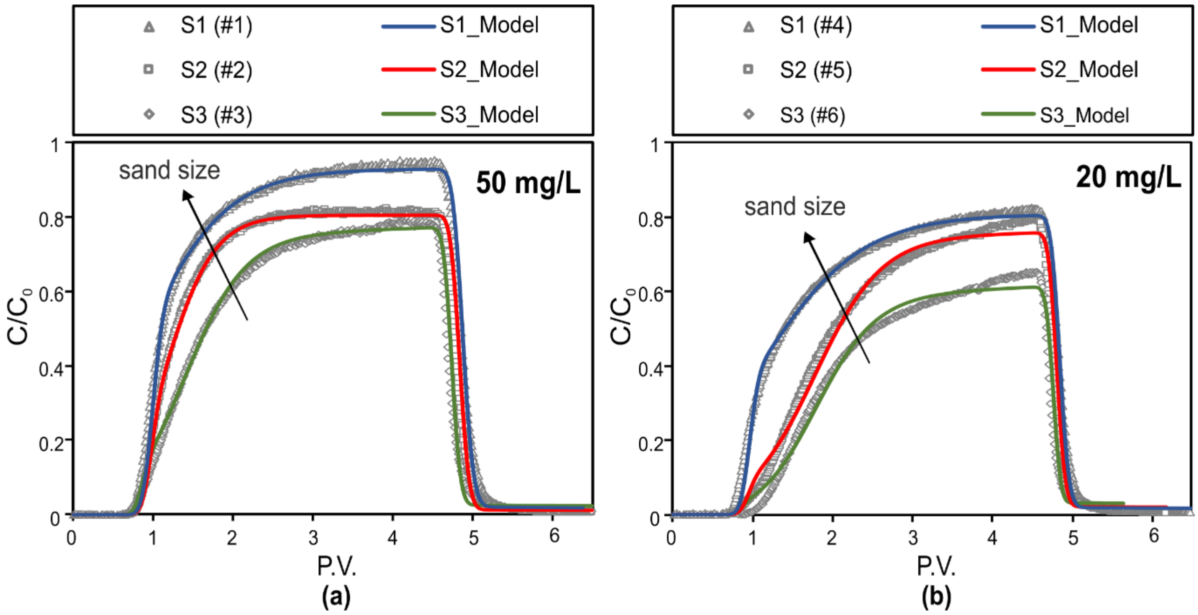

Figure 6: Observed and simulated breakthrough curves for GO_1, injected in columns packed with sand S_1, S_2, and S_3 at a concentration of 50 mg/L and 20 mg/L.

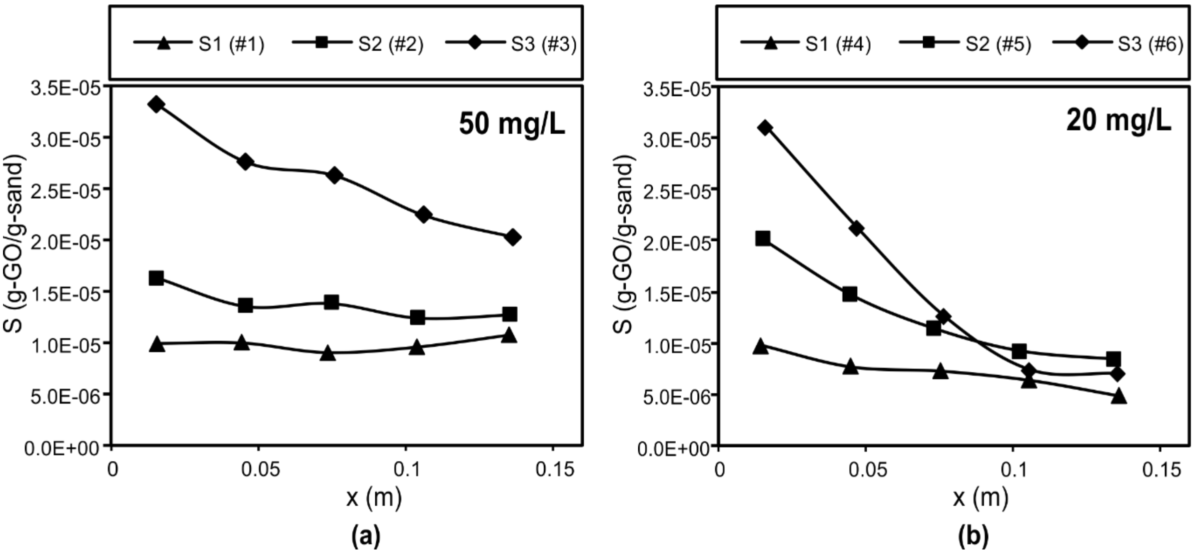

Figure 7: Observed retention profiles of GO_1 with two different input concentrations of (a) 50 mg/L and (b) 20 mg/L in various sand sizes of S_1 (coarse), S_2 (medium), and S_3 (fine).

4. Conclusions

This study showed that GONP can be stably dispersed in water and are remarkably mobile when injected in silica sand. The experimental results also showed that a parameter having a major impact on GONP mobility is the particle lateral size; also the size ratio of particle to sand grains is relevant. Conversely, the source of graphene oxide (i.e. synthesized in the laboratory or provided by commercial producers) had a minor impact, even if the C and O content of the three GONP types was not identical. This suggests that the outcomes of this study could potentially be extended also to other GONP not considered here. The injected concentration affected the mobility of the particles but, at least in the range herein explored, has had no dramatic effect.

Despite the peculiar shape of GONP compared to more conventional colloids, the advection-dispersion-deposition equation commonly used for colloid transport in porous media was still adequate to describe the transport of these particles. The experimental and modeling results indicated that both physico-chemical (blocking) and physical (straining) retention mechanisms strongly influence the transport and retention of GONP. Blocking is observed in all cases and is coherent with the good colloidal stability of the particles. Straining becomes relevant for larger particles and/or finer sand, as expected from round-shaped colloids, and plays a relevant role only for particles exceeding approximately 0.5-1% of the sand d_{10}. Therefore, the retention associated to the physical interaction of GONP with the porous medium cannot be neglected.

Concerning the potential application to groundwater remediation, the results of this study are very promising. GONP are sufficiently mobile to expect a relatively easy injection in the field, and the possibility to control their migration and deposition in the subsoil by modifying the particle size.

5. Acknowledgments

Authors would like to acknowledge prof. Matteo Pavese (DISAT – Politecnico di Torino) and his group for the support in graphene oxide synthesis, and the personnel of laboratories at DIATI - Politecnico di Torino and of the Department of Civil and Environment, Polytechnic University of Tehran (Amirkabir) for their appreciated help with experiments and chemical analyses. The work was conducted in the laboratories of Politecnico di Torino and was partly supported by Iran National Science Foundation (INSF) [grant number 95815221] and Iran Nanotechnology Initiative Council (INIC) [grant number 107029].

6. Competing interests statement

The authors have no competing interests

7. References

Akpotu SO, Moodley B. Application of as-synthesised MCM-41 and MCM-41 wrapped with reduced graphene oxide/graphene oxide in the remediation of acetaminophen and aspirin from aqueous system. Journal of Environmental Management 2018; 209: 205-215.

Bianco C, Tosco T, Sethi R. A 3-dimensional micro- and nanoparticle transport and filtration model (MNM3D) applied to the migration of carbon-based nanomaterials in porous media. Journal of Contaminant Hydrology 2016; 193: 10-20.

Bradford SA, Bettahar M. Concentration dependent transport of colloids in saturated porous media. 2006; 82: 99-117.

Bradford SA, Bettahar M, Simunek J, van Genuchten MT. Straining and Attachment of Colloids in Physically Heterogeneous Porous Media. Vadose Zone Journal 2004; 3: 384-394.

Bradford SA, Kim HN, Haznedaroglu BZ, Torkzaban S, Walker SL. Coupled Factors Influencing Concentration-Dependent Colloid Transport and Retention in Saturated Porous Media. 2009; 43: 6996-7002.

Bradford SA, Simunek J, Bettahar M, Van Genuchten MT, Yates SR. Modeling Colloid Attachment, Straining, and Exclusion in Saturated Porous Media. 2003.

Brovelli A, Malaguerra F, Barry DA. Bioclogging in porous media: Model development and sensitivity to initial conditions. Environmental Modelling & Software 2009; 24: 611-626.

Camesano TA, Logan BE. Influence of Fluid Velocity and Cell Concentration on the Transport of Motile and Nonmotile Bacteria in Porous Media. 1998: 1699-1708.

Chen D, Feng H, Li J. Graphene oxide: preparation, functionalization, and electrochemical applications. Chem Rev 2012; 112: 6027-53.

Chen J, Yao B, Li C, Shi G. An improved Hummers method for eco-friendly synthesis of graphene oxide. Carbon 2013; 64: 225-229.

Chrysikopoulos CV, Sotirelis NP, Kallithrakas-Kontos NG. Cotransport of Graphene Oxide Nanoparticles and Kaolinite Colloids in Porous Media. Transport in Porous Media 2017; 119: 181-204.

Corsi I, Winther-nielsen M, Sethi R, Punta C, Torre CD, Libralato G, et al. Ecofriendly nanotechnologies and nanomaterials for environmental applications : Key issue and consensus recommendations for sustainable and ecosafe nanoremediation. Ecotoxicology and Environmental Safety 2018; 154: 237-244.

Dong S, Gao B, Sun Y, Guo H, Wu J, Cao S, et al. Visualization of graphene oxide transport in two-dimensional homogeneous and heterogeneous porous media. Journal of Hazardous Materials 2019; 369: 334-341.

Dong S, Shi X, Gao B, Wu J, Sun Y, Guo H, et al. Retention and Release of Graphene Oxide in Structured Heterogeneous Porous Media under Saturated and Unsaturated Conditions. Environmental Science & Technology 2016; 50: 10397-10405.

Dong S, Sun Y, Gao B, Shi X, Xu H, Wu J, et al. Retention and transport of graphene oxide in water-saturated limestone media. Chemosphere 2017; 180: 506-512.

Fan W, Jiang X, Lu Y, Huo M, Lin S, Geng Z. Effects of surfactants on graphene oxide nanoparticles transport in saturated porous media. Journal of Environmental Sciences (China) 2015a; 35: 12-19.

Fan W, Jiang XH, Yang W, Geng Z, Huo MX, Liu ZM, et al. Transport of graphene oxide in saturated porous media: Effect of cation composition in mixed Na–Ca electrolyte systems. Science of The Total Environment 2015b; 511: 509-515.

Feriancikova L, Xu S. Deposition and remobilization of graphene oxide within saturated sand packs. Journal of Hazardous Materials 2012; 235-236: 194-200.

Godinez IG, Darnault CJG. Aggregation and transport of nano-TiO2 in saturated porous media: Effects of pH, surfactants and flow velocity. Water Research 2011; 45: 839-851.

Hosseini SM, Tosco T. Transport and retention of high concentrated nano-Fe/Cu particles through highly flow-rated packed sand column. Water Research 2013; 47: 326-338.

Hu Z, Zhao J, Gao H, Nourafkan E, Wen D, Hu Z, et al. Transport and Deposition of Carbon Nanoparticles in Saturated Porous Media. Energies 2017; 10: 1151.

Huang X, Yin Z, Wu S, Qi X, He Q, Zhang Q, et al. Graphene-based materials: Synthesis, characterization, properties, and applications. Small 2011; 7: 1876-1902.

Iqbal MZ, Abdala AA. Oil spill cleanup using graphene. 2013: 3271-3279.

Jian-Zhou H, Cheng-Cheng L, Deng-Jun W, Zhou D-M. Biofilms and extracellular polymeric substances mediate the transport of graphene oxide nanoparticles in saturated porous media. Journal of Hazardous Materials 2015; 300: 467-474.

Jiang Y, Zhang X, Yin X, Sun H, Wang N. Graphene oxide-facilitated transport of Pb2+and Cd2+in saturated porous media. Science of the Total Environment 2018; 631-632: 369-376.

Johnson PR, Sun N, Elimelech M. Colloid transport in physically and geochemically heterogeneous porous media_ Modeling, measurements, and parameter identification.pdf. Environmental Science and Technology 1996; 30: 3284-3293.

Karn B, Kuiken T, Otto M. Nanotechnology and in Situ Remediation : A Review of the Benefits and. 2009; 117: 1823-1831.

Kasel D, Bradford SA, Klumpp E, Gru P. Transport and retention of multi-walled carbon nanotubes in saturated porous media : Effects of input concentration and grain size. 2012; 7.

Lanphere JD, Luth CJ, Walker SL. Effects of Solution Chemistry on the Transport of Graphene Oxide in Saturated Porous Media. Environmental Science & Technology 2013; 47: 4255-4261.

Lanphere JD, Rogers B, Luth C, Bolster CH, Walker SL. Stability and Transport of Graphene Oxide Nanoparticles in Groundwater and Surface Water. Environ Eng Sci 2014; 31: 350-359.

Li Y, Yang N, Du T, Wang X, Chen W. Transformation of graphene oxide by chlorination and chloramination: Implications for environmental transport and fate. Water Res 2016; 103: 416-423.

Liang Y, Bradford SA, Simunek J, Vereecken H, Klumpp E. Sensitivity of the transport and retention of stabilized silver nanoparticles to physicochemical factors. Water Research 2013; 47: 2572-2582.

Liu J, Cui L, Losic D. Graphene and graphene oxide as new nanocarriers for drug delivery applications. Acta Biomaterialia 2013a; 9: 9243-9257.

Liu L, Gao B, Wu L, Morales VL, Yang L, Zhou Z, et al. Deposition and transport of graphene oxide in saturated and unsaturated porous media. Chemical Engineering Journal 2013b; 229: 444-449.

Liu L, Gao B, Wu L, Yang L, Zhou Z, Wang H. Effects of pH and surface metal oxyhydroxides on deposition and transport of carboxyl-functionalized graphene in saturated porous media. Journal of Nanoparticle Research 2013c; 15.

Lotya M, Rakovich A, Donegan JF, Coleman JN. Measuring the lateral size of liquid-exfoliated nanosheets with dynamic light scattering. Nanotechnology 2013; 24.

Lu T, Xia T, Qi Y, Chengdong Z, Chen W. Effect of clay materials on transport of graphene oxide in saturated porous media. 2017; 36: 655-660.

Malgaresi G, Collins B, Alvaro P, Bedrikovetsky P. Explaining non-monotonic retention profiles during flow of size-distributed colloids. Chemical Engineering Journal 2019; 375: 121984.

Messina F, Tosco T, Sethi R. On the failure of upscaling the single-collector efficiency to the transport of colloids in an array of collectors. Water Resources Research 2016; 52: 5492-5505.

Montes-Navajas P, Asenjo NG, Santamaría R, Menéndez R, Corma A, García H. Surface area measurement of graphene oxide in aqueous solutions. Langmuir 2013; 29: 13443-13448.

Novoselov KS, Fal VI, Colombo L, Gellert PR, Schwab MG, Kim K. REVIEW A roadmap for graphene. Nature 2012; 490: 192-200.

O'Carroll D, Sleep B, Krol M, Boparai H, Kocur C. Nanoscale zero valent iron and bimetallic particles for contaminated site remediation. Advances in Water Resources 2013; 51: 104-122.

Patil SS, Shedbalkar UU, Truskewycz A, Chopade BA, Ball AS. Environmental Technology & Innovation Nanoparticles for environmental clean-up : A review of potential risks and emerging solutions. Environmental Technology & Innovation 2016; 5: 10-21.

Paulchamy B, Arthi G, Lignesh B. A Simple Approach to Stepwise Synthesis of Graphene Oxide Nanomaterial. Journal of Nanomedicine & Nanotechnology 2015; 06: 2-5.

Peng S, Wu D, Ge Z, Tong M, Kim H. Influence of graphene oxide on the transport and deposition behaviors of colloids in saturated porous media. Environmental Pollution 2017; 225: 141-149.

Qi Z, Zhang L, Chen W. Transport of graphene oxide nanoparticles in saturated sandy soil. Environmental Sciences: Processes and Impacts 2014a; 16: 2268-2277.

Qi Z, Zhang L, Wang F, Hou L, Chen W. Factors controlling transport of graphene oxide nanoparticles in saturated sand column. 2014b; 33: 998-1004.

Rittman BE. The effect of shear stress on biofilm loss rate. Biotechnology and Bioengineering 1982; 24: 501-506.

Shahriary L, Athawale AA. Graphene Oxide Synthesized by using Modified Hummers Approach. International Journal of Renewable Energy and Environmental Engineering 2014; 02: 58-63.

Sun L, Yu H, Fugetsu B. Graphene oxide adsorption enhanced by in situ reduction with sodium hydrosulfite to remove acridine orange from aqueous solution. Journal of Hazardous Materials 2012; 203-204: 101-110.

Sun Y, Gao B, Bradford SA, Wu L, Chen H, Shi X, et al. Transport, retention, and size perturbation of graphene oxide in saturated porous media: Effects of input concentration and grain size. Water Research 2015; 68: 24-33.

Torkzaban S, Kim Y, Mulvihill M, Wan J, Tokunaga TK. Transport and deposition of functionalized CdTe nanoparticles in saturated porous media. Journal of Contaminant Hydrology 2010; 118: 208-217.

Tortello M, Colonna S, Bernal M, Gomez J, Pavese M, Novara C, et al. Effect of thermal annealing on the heat transfer properties of reduced graphite oxide flakes: A nanoscale characterization via scanning thermal microscopy. Carbon 2016; 109: 390-401.

Tosco T, Bosch J, Meckenstock RU, Sethi R. Transport of ferrihydrite nanoparticles in saturated porous media: Role of ionic strength and flow rate. Environmental Science and Technology 2012; 46: 4008-4015.

Tosco T, Petrangeli M, Cruz C, Sethi R. Nanoscale zerovalent iron particles for groundwater remediation : a review. Journal of Cleaner Production 2014; 77: 10-21.

Tosco T, Sethi R. Transport of non-newtonian suspensions of highly concentrated micro- and nanoscale iron particles in porous media: A modeling approach. Environmental Science and Technology 2010; 44: 9062-9068.

Tosco T, Tiraferri A, Sethi R. Ionic Strength Dependent Transport of Microparticles in Saturated Porous Media: Modeling Mobilization and Immobilization Phenomena under Transient Chemical Conditions. Environmental Science & Technology 2009; 43: 4425-4431.

Tufenkji N, Elimelech M. Correlation Equation for Predicting Single-Collector Efficiency in Physicochemical Filtration in Saturated Porous Media. 2004; 38: 529-536.

Wang C, Bobba AD, Attinti R, Shen C, Lazouskaya V, Wang L-P, et al. Retention and Transport of Silica Nanoparticles in Saturated Porous Media: E ff ect of Concentration and Particle Size. 2012.

Wang D, Paradelo M, Bradford SA, Peijnenburg WJGM, Chu L, Zhou D. Facilitated transport of Cu with hydroxyapatite nanoparticles in saturated sand: Effects of solution ionic strength and composition. Water Research 2011; 45: 5905-5915.

Wang M, Gao B, Tang D, Sun H, Yin X, Yu C. Effects of temperature on graphene oxide deposition and transport in saturated porous media. J Hazard Mater 2017; 331: 28-35.

Wang M, Gao B, Tang D, Yu C. Concurrent aggregation and transport of graphene oxide in saturated porous media : Roles of temperature , cation type , and electrolyte. Environmental Pollution 2018; 235: 350-357.

Xia T, Qi Y, Zhu L, Qi Z, Chen W. Transport and retention of reduced graphene oxide materials in saturated porous media : Synergistic effects of enhanced attachment and particle aggregation *. 2019; 247: 383-391.

Xu S, Gao B, Saiers JE. Straining of colloidal particles in saturated porous media. Water Resources Research 2006; 42.

Yang X, Li J, Wen T, Ren X, Huang Y, Wang X. Colloids and Surfaces A : Physicochemical and Engineering Aspects Adsorption of naphthalene and its derivatives on magnetic graphene composites and the mechanism investigation. Colloids and Surfaces A: Physicochemical and Engineering Aspects 2013; 422: 118-125.

Yao K-M, Habibian MT, O'Melia CR. Water and Waste Water Filtration: Concepts and Applications. 1971; 5: 1105-1112.

Yin X, Jiang Y, Tan Y, Meng X, Sun H, Wang N. Co-transport of graphene oxide and heavy metal ions in surface-modified porous media. Chemosphere 2019; 218: 1-13.

Zhang W, Morales VnL, Cakmak ME, Salvucci AE, Geohring LD, Hay AG, et al. Colloid Transport and Retention in Unsaturated Porous Media: Effect of Colloid Input Concentration. Environmental Science & Technology 2010; 44: 4965-4972.

Zhao K, Chen C, Cheng T, Shang J. Graphene oxide-facilitated uranium transport and release in saturated medium : Effect of ionic strength and medium structure. Environmental Pollution 2019; 247: 668-677.

Zhou DD, Jiang XH, Lu Y, Fan W, Huo MX, Crittenden JC. Cotransport of graphene oxide and Cu(II) through saturated porous media. Science of the Total Environment 2016; 550: 717-726.